

See discussions, stats, and author profiles for this publication at: <https://www.researchgate.net/publication/281437905>

Effect of the Degree of Hydrogen Bonding on Asymmetric Lamellar Microdomains in Binary Block Copolymer Blends

ARTICLE *in* MACROMOLECULES · AUGUST 2015

Impact Factor: 5.8

READS

9

1 AUTHOR:



Sung Hyun Han

Samsung Advanced Institute of Technology

15 PUBLICATIONS 185 CITATIONS

[SEE PROFILE](#)

Effect of the Degree of Hydrogen Bonding on Asymmetric Lamellar Microdomains in Binary Block Copolymer Blends

Jongheon Kwak, Sung Hyun Han, Hong Chul Moon, and Jin Kon Kim*

National Creative Research Initiative Center for Smart Block Copolymers, Department of Chemical Engineering, Pohang University of Science and Technology, Pohang, Kyungbuk 790-784, Republic of Korea

Victor Pryamitsyn and Venkat Ganesan

Department of Chemical Engineering, University of Texas at Austin, Austin, Texas 78712, United States

Supporting Information

1. INTRODUCTION

Block copolymers have attracted significant interest for their ability to form uniformly repeated microdomain structures such as lamellae, cylinders, gyroids, and spheres. The resulting morphologies could be tuned, depending on the volume fraction (f) of one block, the degree of polymerization (N), and the Flory–Huggins segmental interaction parameter (χ).^{1–4} Among these morphologies, lamellar structures with tunable microdomain periods have received considerable attention for various applications such as photonic crystals and next-generation lithography.^{5–9} However, conventional AB diblock copolymers exhibit lamellar structures only when the volume fraction of each block is almost equal^{10–12} and hence cannot produce highly asymmetric lamellar morphology, which may be desirable for some applications. For finding unusual nanostructures that cannot be obtained by neat block copolymers, many research groups have employed blend system of block copolymers.^{13–19}

Recently, we reported the creation of highly asymmetric lamellar structure by using binary blends consisting of high molecular weight of asymmetric polystyrene-*block*-poly(2-vinylpyridine) copolymer (as-PS-*b*-P2VP) and low molecular weight of asymmetric polystyrene-*block*-poly(4-hydroxystyrene) copolymer (as-PS-*b*-PHS). Although neat as-PS-*b*-P2VP and as-PS-*b*-PHS have body-centered cubic (BCC) spherical microdomains, the morphology of the binary blend showed highly asymmetric lamellar structure due to the interface curvature changes arising from the favorable hydrogen bonding interaction between P2VP and PHS chains. Since the volume fraction of PS microdomain in the blend was 0.8, the ratio of PS and (P2VP + PHS) lamellar width is 4, confirmed by small-angle X-ray scattering (SAXS) and transmission electron microscopy (TEM).^{20,21}

Very recently, Shi et al.^{22,23} reported that an extremely asymmetric lamellar structure with up to ~97 wt % of one block by using binary mixture of a miktoarm star block copolymer [S(IS')₃, here S and I denote PS and polyisoprene, respectively] and suitable choice of molecular weight of PS homopolymer. Although S(IS')₃ stabilized extremely asymmetric lamellar structure even at large amount of PS homopolymer, the resulting microdomains do not show long-range ordering, resulting in nonuniform lamellar spacing throughout the entire area.

Thus, there is still a need for strategies which can result in well-defined and highly asymmetric lamellae with larger lamellar width ratio compared with that (~4) reported in our previous study.²⁰ Since asymmetric lamellar microdomains are formed due to the interface curvature change by favorable hydrogen bonding interaction between the hydroxyl group and nitrogen atom, a large ratio of lamellar width (thus, enhanced asymmetry) could potentially be achieved by increasing the degree of the hydrogen bonding. Poly(4-vinylpyridine) (P4VP) is a model polymer that exhibits much stronger hydrogen bonding with PHS compared with P2VP.²⁴ Thus, we hypothesize that when PS-*b*-P4VP is used instead of PS-*b*-P2VP, it would achieve lamellae with larger asymmetries. Furthermore, since PS-*b*-P4VP has higher χ (0.3) than that (0.1) of PS-*b*-P2VP,^{25,26} the microdomains could be obtained even at lower molecular weights of PS-*b*-P4VP. In this situation, the resulting microdomains are likely to possess sub-10 nm lamellar widths and could likely be of significant interest for developing next-generation lithography techniques.

On the basis of the above hypothesis, in this study, we compared the phase transformation to asymmetric lamellae of two binary block copolymer mixtures: as-PS-*b*-P4VP/as-PS-*b*-PHS and as-PS-*b*-P2VP/as-PS-*b*-PHS. It was confirmed by SAXS and TEM that the as-PS-*b*-P4VP/as-PS-*b*-PHS blend showed enhanced asymmetric lamellar microdomains having lamellar width ratio of 6:1, which is 50% increase of that (4:1) obtained by the as-PS-*b*-P2VP/as-PS-*b*-PHS blend. Moreover, by using the as-PS-*b*-P4VP/as-PS-*b*-PHS blend, we could decrease the width of P4VP + PHS lamellar microdomain down to ~5 nm. To explain the effect of hydrogen bonding on the asymmetric lamellar morphology, we used the strong stretching theory (SST) model developed in our previous work.²⁷ Qualitatively consistent with the experimental results, the SST model predicts that the formation of asymmetric lamellar morphology depends on the degree of favorable interaction between B and C blocks.

Received: July 13, 2015

Revised: August 10, 2015

2. EXPERIMENTAL SECTION

Materials. Asymmetric PS-*b*-P4VP and PS-*b*-P2VP were purchased from Polymer Source. Three as-PS-*b*-PHS with various volume fractions of PS were prepared by the hydrolysis of polystyrene-*block*-poly(4-*tert*-butoxystyrene) copolymers (PS-*b*-PtBOS), which were synthesized by sequential anionic polymerization in tetrahydrofuran (THF) at -78 °C under an argon environment using *sec*-butyllithium (*s*-BuLi) as an initiator.²⁰ Binary blends of 50:50 (w/w) as-PS-*b*-P4VP/as-PS-*b*-PHS and as-PS-*b*-P2VP/as-PS-*b*-PHS were prepared by using a cosolvent of dimethylformamide (DMF) and solution cast from 10 wt % DMF solution and dried at 80 °C. For the complete removal of DMF, all samples were thermally annealed at 180 °C for 5 days under vacuum and quenched at room temperature.

Molecular Characterization. The number-average molecular weight (M_n) and polydispersity index (PDI) of as-PS-*b*-PHS were measured by size exclusion chromatography (SEC: Waters 2414 refractive index detector) based on PS standards. Two 300 mm (length) × 7.5 mm (inner diameter) columns including particle size of 5 μm (PLgel 5 μm MIXED-C: Polymer Laboratories) were used with THF as an eluent and a flow rate of 1 mL/min at 30 °C. The volume fraction of PS (f_{PS}) was determined by ¹H nuclear magnetic resonance spectra (¹H NMR: Bruker Avance III 400) with a solvent of acetone-*d* ((CD₃)₂CO). The microdomains of all neat block copolymers were investigated by SAXS and TEM (see section 1 of the Supporting Information). The molecular characteristics of all the samples are summarized in Table 1.

Table 1. Molecular Characteristics of Polymers Employed in This Study

sample	M_n (g/mol)	M_w/M_n	f_{PS}^b	microdomains ^c
as-S4VP-1	34000	1.15	0.81	cylinder
as-S4VP-2	56000	1.09	0.9	spheres
as-S4VP-3	64000	1.1	0.94	spheres
as-S2VP-1	63000	1.07	0.79	cylinder
as-S2VP-2	63000	1.1	0.88	spheres
as-S2VP-3	106000	1.07	0.83	spheres
as-SHS-1	23000 ^a	1.10 ^a	0.82	spheres
as-SHS-2	24000 ^a	1.10 ^a	0.91	spheres
as-SHS-3	21000 ^a	1.06 ^a	0.93	spheres
as-S4VP-1/as-SHS-1				lamellar
as-S4VP-2/as-SHS-1				lamellar
as-S4VP-3/as-SHS-1				cylinder
as-S2VP-1/as-SHS-1				lamellar
as-S2VP-2/as-SHS-1				cylinder
as-S2VP-3/as-SHS-1				lamellar
as-S4VP-2/as-SHS-2				cylinder
as-S4VP-2/as-SHS-3				cylinder (poor ordering)

^a M_n and M_w are the number- and weight-average molecular weights measured by SEC based on PS standards. ^b f_{PS} was calculated from the weight fraction of PS and PHS measured by ¹H NMR and known density at room temperature (PS = 1.05 g/cm³, P4VP = 1.15 g/cm³, P2VP = 1.15 g/cm³, PHS = 1.16 g/cm³).^{28,29} ^cMicrodomains of neat block copolymers and binary blends were determined by SAXS and TEM images (Figures 1 and 2; Figures S2 and S3).

Small-Angle X-ray Scattering (SAXS). SAXS profiles [$I(q)$] vs q (= $(4\pi/\lambda) \sin \theta/2$), where q and 2θ are the scattering vector and scattering angle, respectively] were obtained at the in-vacuum Undulator 20 beamline (4C SAXS II) of the Pohang Accelerator Laboratory (PAL) Korea. The wavelength and beam size were 0.675 Å and 0.2 (H) × 0.6 (W) mm², respectively. A two-dimensional charge-coupled detector (Mar USA, Inc.) was employed. The sample-to-detector distance was 4 m. Samples were annealed at 180 °C for 5 days

in a vacuum, followed by quenching at room temperature. The thickness of the samples was 1.0 mm, and the exposure time was 100 s.

Transmission Electron Microscopy (TEM). The samples were ultrasectioned by using a Leica Ultracut Microtome (EM UC6 Leica Ltd.) at room temperature with a thickness of ~40 nm. Then, they were stained by exposure to iodine vapor for 1 h at room temperature. The P4VP (or P2VP) and PHS microdomains look dark in TEM images. The micrographs were taken at room temperature by bright-field TEM (S-7600 Hitachi Ltd.) at 80 kV.

3. RESULTS AND DISCUSSION

Figures 1a and 1c show SAXS profile and TEM image for 50/50 (w/w) as-S4VP-2/as-SHS-1 blend. The SAXS profile (Figure 1a) shows scattering peaks at the position of 1:2:3 relative to q^* (0.1725 nm⁻¹), indicating that as-S4VP-2/as-SHS-1 blend has lamellar microdomains. The domain spacing ($2\pi/q^*$) obtained from SAXS profile was 36 nm, which is consistent with TEM result. In TEM images (Figures 1c and 1d), the bright and dark parts correspond to PS and P4VP (or P2VP)/PHS microdomains, respectively, due to the selective staining of P4VP (or P2VP) and PHS by iodine. The SAXS profile was also analyzed by fitting with a variable lamellar thickness structure model (see section 3 of the Supporting Information). From the fitting, the estimated volume fraction of PS microdomains is 0.86, which is well anticipated by the average volume fraction of PS block (f_{PS}) of as-S4VP-2 and as-SHS-1. The TEM image (Figure 1c) shows that the lamellar width ratio of PS block to P4VP/PHS block in as-S4VP-2/as-SHS-1 blend is 6:1, and the lamellar width of P4VP/PHS microdomain is ~5 nm.

However, when as-S2VP-2 with similar volume fraction of PS block and total molecular weight with as-S4VP-2 is blended with as-SHS-1, this blend shows cylindrical morphology, not lamellar morphology, evident by the SAXS profile (Figure 1b) exhibiting the scattering peaks at the position of 1: $\sqrt{3}$: $\sqrt{4}$: $\sqrt{7}$ relative to q^* . Cylindrical microdomains are also clearly seen in TEM image (Figure 1d). The results given in Figure 1 suggest that the favorable hydrogen bonding interaction between P4VP/PHS, which is a main driving force to induce the phase transformation from BCC spherical microdomains to asymmetric lamellae, is much stronger than P2VP/PHS. Thus, we obtain asymmetric lamellar morphology with increased lamellar width ratio compared with the as-PS-*b*-P2VP/as-PS-*b*-PHS blend.

To enhance the asymmetry of the lamellar microdomains, we increased the volume fraction of PS in as-S4VP (as-S4VP-3) and in as-SHS (as-SHS-2 and as-SHS-3) with similar total molecular weight to as-S4VP-2 and as-SHS-1. Figure 2 gives SAXS profiles and TEM images for three samples: 50/50 (w/w) as-S4VP-3/as-SHS-1 blend, 50/50 (w/w) as-S4VP-2/as-SHS-2 blend, and 50/50 (w/w) as-S4VP-2/as-SHS-3 blend. Contrary to our expectation, all SAXS profiles of three blends show the scattering peaks of 1: $\sqrt{3}$: $\sqrt{4}$ relative to q^* . This indicates that all three blends show cylindrical microdomains, which are also confirmed by TEM images. Thus, the phase transformation from spherical structure to asymmetric lamellae did not occur. It is noted that while as-S4VP-2/as-SHS-2 blend shows distinct cylindrical morphology with good long-range ordering, as-S4VP-2/as-SHS-3 blend shows cylindrical morphology with poor long-range ordering. This is because of the decrease volume fraction of PHS in as-SHS-3 compared with as-SHS-2. It would be obvious that with decreasing PHS molecular weight the chance of the hydrogen bonding formation with P4VP should decrease.

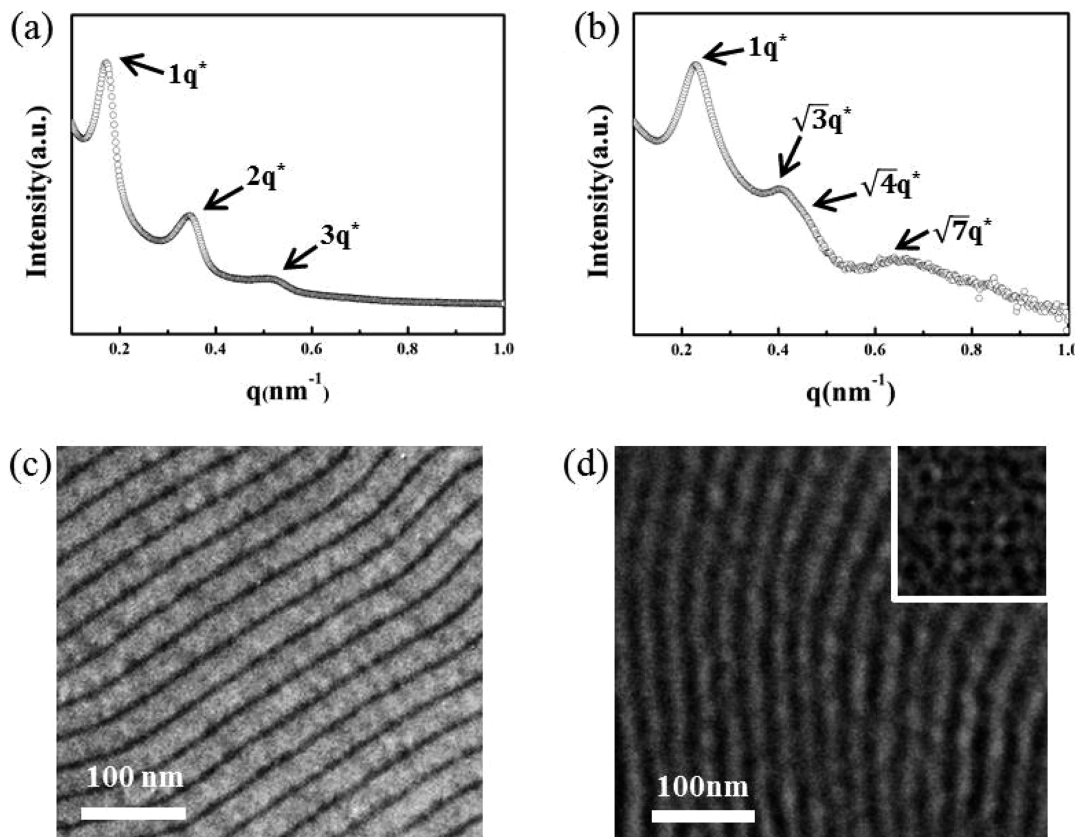


Figure 1. SAXS profile (a) and TEM image (c) for 50/50 (w/w) as-S4VP-2/as-SHS-1 blend. SAXS profile (b) and TEM image (d) for 50/50 (w/w) as-S2VP-2/as-SHS-1 blend.

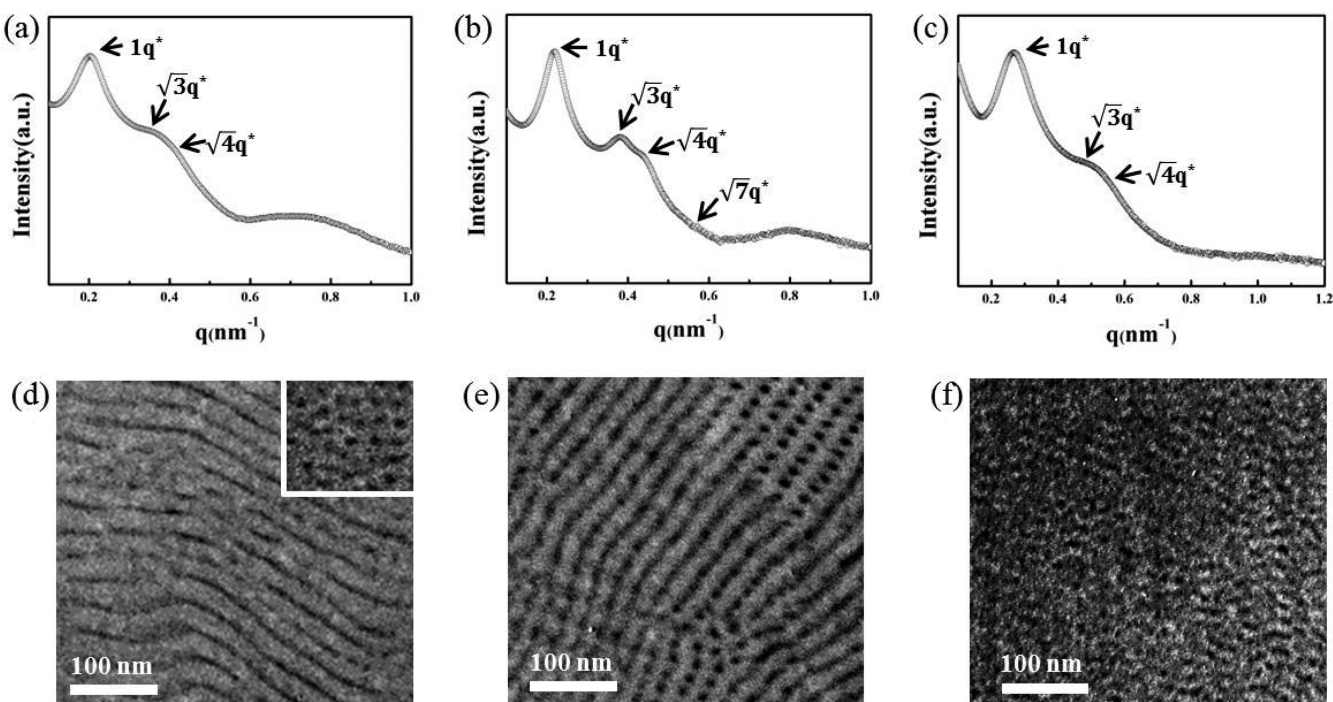


Figure 2. SAXS profile (upper panels) and TEM image (lower panels) for 50/50 (w/w) as-S4VP-3/as-SHS-1 blend (a, d), 50/50 (w/w) as-S4VP-2/as-SHS-2 blend (b, e), and 50/50 (w/w) as-S4VP-2/as-SHS-3 blend (c, f).

From the result given in Figure 1, the as-S4VP-2/as-SHS-1 blend showed asymmetric lamellae at increased f_{PS} compared with the as-S2VP-2/as-SHS-1 blend, even though $\chi_{\text{AB}} \sim 0.3$ of

PS/P4VP is 3 times higher than that (~ 0.1) of PS/P2VP.^{25,26} It is known that with increasing χ_{AB} the phase transformation from sphere to lamellae is harder to occur.²⁰ To overcome this

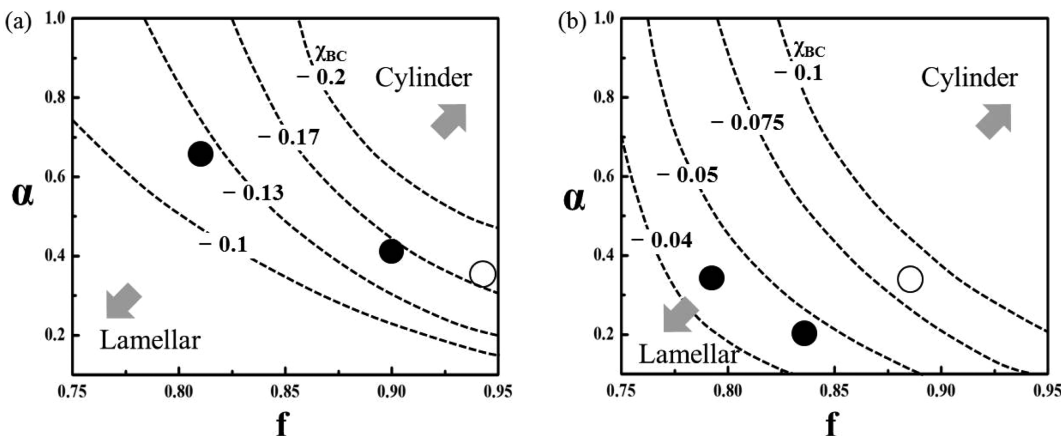


Figure 3. Phase boundary between asymmetric lamellae (lower region) to cylinders (upper region) predicted by the SST model as a function of f and $\alpha (= N_{AC}/N_{AB})$ for (a) as-PS-*b*-P4VP/as-SHS-1 blend and (b) as-PS-*b*-P2VP/as-SHS-1 blend at various values of χ_{BC} . Here, $N_{AC} = 230$, $\chi_{AB}(\text{PS/P4VP}) = 0.3$, $\chi_{AB}(\text{PS/P2VP}) = 0.1$, $f_S = 0.82$, and $w = 0.5$. The experimental data are shown in symbols (filled and open circles represent asymmetric lamellae and cylinders, respectively).

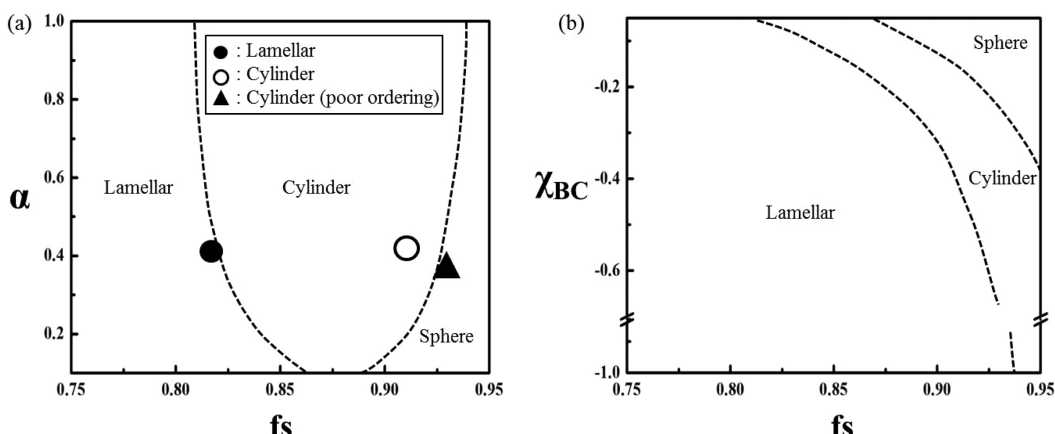


Figure 4. (a) Equilibrium morphology of as-PS-*b*-P4VP/as-PS-*b*-PHS blend predicted by the SST model as a function of α and f_S at given $N_{AC} = 200$, $\chi_{AB} = 0.3$, $\chi_{BC} = -0.17$, $f = 0.9$, and $w = 0.5$. (b) Equilibrium morphology of as-PS-*b*-P4VP/as-PS-*b*-PHS blend predicted by the SST model depending on χ_{BC} and f_S at given $N_{AB} = 2000$, $\chi_{AB} = 0.3$, $f = 0.9$, $\alpha = 0.2$, and $w = 0.5$.

large χ_{AB} for PS/P4VP, the degree of the hydrogen bonding between P4VP and PHS should be higher than that between P2VP and PHS. Unfortunately, it is not easy to experimentally obtain χ_{BC} of P4VP/PHS and P2VP/PHS, although two χ should have negative values and the absolute value ($-\chi$) of P4VP/PHS is larger than that of P2VP/PHS.²⁴

To understand the experimental results and also explore the limits of our strategy, we first estimated these two values by comparing the experimentally observed asymmetric lamellar morphologies with those of predicted results by the SST model.²⁷ According to the SST model,²⁷ the phase behavior of (A-B)/(A-C) binary blend capable of hydrogen bonding between B and C blocks depends on several parameters: (1) the number of segments for AB chains and AC chains denoted as N_{AB} and N_{AC} , respectively; (2) the volume fractions of A in AB and AC chains defined by $f = N_A/N_{AB}$ and $f_S = N_A/N_{AC}$ (N_A is the number of segments for A chain (here PS block) in AB and AC chains); and (3) the Flory-Huggins interaction parameters between A/B, A/C, and B/C segments denoted as χ_{AB} , χ_{AC} , and χ_{BC} , respectively. In this study, we fixed the amount of AC chains in the binary blend (w) as 0.5.

Figure 3 shows the predicted equilibrium morphologies as a function of f and $\alpha (= N_{AC}/N_{AB})$ for as-PS-*b*-P4VP/as-SHS-1 blend (Figure 3a) and as-PS-*b*-P2VP/as-SHS-1 blend (Figure

3b) at various χ_{BC} values. Here, as-SHS-1 ($N_{AC} = 230$, $f_S = 0.82$) was used for both blends. It is noted that as-S4VP-1/as-SHS-1, as-S2VP-1/as-SHS-1, and as-S2VP-3/as-SHS-1 blends which have less asymmetric volume fraction showed asymmetric lamellar morphologies (see section 2 of the Supporting Information). By comparison between the experimentally observed microdomains with the predicted ones, χ_{BC} of P4VP/PHS is estimated to ~ -0.17 , while χ_{BC} of P2VP/PHS has a value between -0.05 and -0.075 . The large negative value of P4VP/PHS compared with P2VP/PHS is consistent with the experimental result that the favorable hydrogen bonding between P4VP/PHS is greater than that of P2VP/PHS.²⁴ This is because the hydroxyl group (OH) in the para (or 4-) position of PHS could have greater interassociation with nitrogen atom located in the para (or 4-) position of pyridine unit than P2VP. On the other hand, since P2VP has a nitrogen atom located in the ortho (or 2-) position of pyridine unit, interassociation between N and OH groups would be hindered. As a result, the greater interassociation force (or higher $-\chi$ value) between P4VP/PHS of as-PS-*b*-P4VP/as-PS-*b*-PHS blend enables phase transformation to asymmetric lamellae to occur at more asymmetric condition (increased PS volume fraction) compared with the as-PS-*b*-P2VP/as-PS-*b*-PHS blend.

Furthermore, both as-PS-*b*-P4VP/as-SHS-1 and as-PS-*b*-P2VP/as-SHS-1 blends show the same tendency that lamellar microdomains are easily formed as α decreases. The smaller α represents increased N_{AB} due to the fixed N_{AC} . In this situation, PHS chains should be more stretched, while P4VP (or P2VP) chains are more compressed, to maximize the hydrogen bonding (or intermixing) between P4VP (or P2VP) and PHS segments, which results in increased curvature modification.

Using the estimated interaction parameter of P4VP/PHS, we consider the effect of f_S (the volume fraction of PS in as-PS-*b*-PHS) on the formation of asymmetric lamellar structure as a function of α at a given $f = 0.90$. Here, $N_{AC} = 200$, $\chi_{AB} = 0.3$, $\chi_{BC} = -0.17$, and $w = 0.5$. Figure 4a shows that for $\alpha = 0.4$ (corresponding to as-S4VP-2) the phase boundary for f_S to form asymmetric lamellar structure is ~ 0.82 . This is consistent with the experimental result that the blend of as-S4VP-2/as-SHS-1 with $f_S = 0.82$ showed asymmetric lamellae (see Figure 1a). The cylindrical morphology observed in the blend of as-S4VP-2/as-SHS-2 with $f_S = 0.91$ (see Figure 2b) is also well-matched with the theoretical predictions. However, we recall that the blend of as-S4VP-2/as-SHS-3 with $f_S = 0.93$ showed cylinders with poor long-range ordering (see Figure 2c). In contrast, the theory predicts spherical morphology, though the boundary to cylinders is close to such conditions. The discrepancy between experimental and predicted morphology for the blend of as-S4VP-2/as-SHS-3 may be rationalized by noting that the SST model is approximate in nature and ignores many scaling factors of the order unity. Hence, phase behavior differences arising from slight changes in the free energy may not be captured within such a model. Moreover, other sources of error, for instance, the accuracy of the parametrization of $-\chi_{BC}$, also contribute as a potential source of error.

Nevertheless, the experimental results show qualitative agreement with the SST model predictions and confirm our hypothesis that the ability to achieve highly asymmetric lamellae was facilitated by tuning the H-bonding interactions.

Finally, the SST model suggests that even very large asymmetric lamellar structure (for instance, the lamellar width ratio with 10:1) may be achievable by changing χ_{BC} . For this purpose, we used $N_{AB} = 2000$, $\chi_{AB} = 0.3$, $f = 0.9$, $\alpha = 0.2$, and $w = 0.5$. Figure 4b shows that at $\chi_{BC} \sim -0.65$ the range of f_S forming lamellar structure is expanded up to 0.925, which corresponds to asymmetric lamellae with the lamellar width ratio of 10:1. Thus, with increasing very large intermolecular force between B and C blocks through using multiple hydrogen bonding interactions (for instance, quadruple hydrogen bonding), one can even achieve extremely large asymmetric lamellar morphology. This is an interesting direction for a future study.

4. CONCLUSIONS

We have investigated the phase behavior of (A-B)/(A-C) binary blends capable of hydrogen bonding between B and C blocks, focusing on the degree of hydrogen bonding power. Two kinds of binary blends (PS-*b*-P4VP/PS-*b*-PHS and PS-*b*-P2VP/PS-*b*-PHS) were employed. It was observed by SAXS and TEM that the PS-*b*-P4VP/PS-*b*-PHS blend formed asymmetric lamellar morphology at more asymmetric volume fraction where PS-*b*-P2VP/PS-*b*-PHS blend could not form. By comparing the experimentally observed morphology with theoretically predicted morphology by the SST model, we estimated χ of P4VP/PHS to be ~ -0.17 and χ of P2VP/PHS to have a value between -0.05 and -0.075 . This is consistent

with the fact that the favorable hydrogen bonding between P4VP/PHS was greater than that of P2VP/PHS. From the SST model, extremely large asymmetric lamellar morphology (say the lamellar width ratio greater than 10:1) could be achieved when very large favorable intermolecular force between B and C blocks (for instance, multiple hydrogen bonding) is introduced.

■ ASSOCIATED CONTENT

S Supporting Information

The Supporting Information is available free of charge on the ACS Publications website at DOI: 10.1021/acs.macromol.5b01546.

SEC chromatogram, NMR spectra, SAXS profiles and TEM images for neat block copolymers; SAXS profiles for binary blends; fitting data of SAXS profile with a variable lamellar thickness structure model (PDF)

■ AUTHOR INFORMATION

Corresponding Author

*E-mail jkkim@postech.ac.kr (J.K.K.).

Present Address

H.C.M.: Department of Chemical Engineering, University of Seoul, Seoul 130-743, Republic of Korea.

Notes

The authors declare no competing financial interest.

■ ACKNOWLEDGMENTS

This work was supported by the National Creative Research Initiative Program supported by the National Research Foundation of Korea (2013R1A3A2042196). The SAXS experiment was done at 4C beamline of PAL (Korea). V.G. and V.P. were supported in part by grants from Robert A. Welch Foundation (Grant F1599) and National Science Foundation (DMR-1306844) and the US Army Research Office under Grant W911NF-13-1-0396.

■ REFERENCES

- (1) Leibler, L. *Macromolecules* **1980**, *13*, 1602–1617.
- (2) Bates, F. S.; Fredrickson, G. H. *Annu. Rev. Phys. Chem.* **1990**, *41*, 525–557.
- (3) Kim, J. K.; Lee, J. I.; Lee, D. H. *Macromol. Res.* **2008**, *16*, 267–292.
- (4) Kim, J. K.; Yang, S. Y.; Lee, Y.; Kim, Y. *Prog. Polym. Sci.* **2010**, *35*, 1325–1349.
- (5) Kang, C.; Kim, E.; Baek, H.; Hwang, K.; Kwak, D.; Kang, Y.; Thomas, E. L. *J. Am. Chem. Soc.* **2009**, *131*, 7538–7539.
- (6) Moonen, P. F.; Yakimets, I.; Huskens, J. *Adv. Mater.* **2012**, *24*, 5526–5541.
- (7) Carlson, A.; Bowen, A. M.; Huang, Y.; Nuzzo, R. G.; Rogers, J. A. *Adv. Mater.* **2012**, *24*, 5284–5318.
- (8) Lee, J.-H.; Koh, C. Y.; Singer, J. P.; Jeon, S.-J.; Maldovan, M.; Stein, O.; Thomas, E. L. *Adv. Mater.* **2014**, *26*, 532–569.
- (9) Macfarlane, R. J.; Kim, B.; Lee, B.; Weitekamp, R. A.; Bates, C. M.; Lee, S. F.; Chang, A. B.; Delaney, K. T.; Fredrickson, G. H.; Atwater, H. A.; Grubbs, R. H. *J. Am. Chem. Soc.* **2014**, *136*, 17374–17377.
- (10) Khandpur, A. K.; Förster, S.; Bates, F. S.; Hamley, I. W.; Ryan, A. J.; Bras, W.; Almdal, K.; Mortensen, K. *Macromolecules* **1995**, *28*, 8796–8806.
- (11) Kim, J. K.; Han, C. D. *Adv. Polym. Sci.* **2010**, *231*, 77–145.
- (12) Matsen, M. W. *Macromolecules* **2012**, *45*, 2161–2165.
- (13) Moon, H. C.; Han, S. H.; Kim, J. K.; Li, G. H.; Cho, J. *Macromolecules* **2008**, *41*, 6793–6799.

- (14) Moon, H. C.; Han, S. H.; Kim, J. K.; Cho, J. *Macromolecules* **2009**, *42*, 5406–5410.
- (15) Dobrosielska, K.; Takano, A.; Matsushita, Y. *Macromolecules* **2010**, *43*, 1101–1107.
- (16) Matsushita, Y.; Noro, A.; Takano, A. *Polym. J.* **2012**, *44*, 72–82.
- (17) Moon, H. C.; Kim, J. G.; Kim, J. K. *Macromolecules* **2012**, *45*, 3639–3643.
- (18) Moon, H. C.; Kim, J. K. *Polymer* **2013**, *54*, 5437–5442.
- (19) Moon, H. C.; Li, C.; Han, S. H.; Kwak, J.; Kim, J. K. *Polymer* **2014**, *55*, 951–957.
- (20) Han, S. H.; Pryamitsyn, V.; Bae, D.; Kwak, J.; Ganesan, V.; Kim, J. K. *ACS Nano* **2012**, *6*, 7966–7972.
- (21) Kwak, J.; Han, S. H.; Moon, H. C.; Kim, J. K.; Koo, J.; Lee, J.; Pryamitsyn, V.; Ganesan, V. *Macromolecules* **2015**, *48*, 1262–1266.
- (22) Shi, W.; Lynd, N. A.; Montarnal, D.; Luo, Y.; Fredrickson, G. H.; Kramer, E. J.; Ntaras, C.; Avgeropoulos, A.; Hexemer, A. *Macromolecules* **2014**, *47*, 2037–2043.
- (23) Shi, W.; Hamilton, A. L.; Delaney, K. T.; Fredrickson, G. H.; Kramer, E. J.; Ntaras, C.; Avgeropoulos, A.; Lynd, N. A. *J. Am. Chem. Soc.* **2015**, *137*, 6160–6163.
- (24) Kuo, S. W.; Lin, C. L.; Chang, F. C. *Polymer* **2002**, *43*, 3943–3949.
- (25) Alberda van Ekenstein, G. O. R.; Meyboom, R.; ten Brinke, G.; Ikkala, O. *Macromolecules* **2000**, *33*, 3752–3756.
- (26) Zha, W.; Han, C. D.; Lee, D. H.; Han, S. H.; Kim, J. K.; Kang, J. H.; Park, C. *Macromolecules* **2007**, *40*, 2109–2119.
- (27) Pryamitsyn, V.; Han, S. H.; Kim, J. K.; Ganesan, V. *Macromolecules* **2012**, *45*, 8729–8742.
- (28) Han, S. H.; Kim, J. K.; Pryamitsyn, V.; Ganesan, V. *Macromolecules* **2011**, *44*, 4970–4976.
- (29) Krawicz, A.; Yang, J.; Anzenberg, E.; Yano, J.; Sharp, I. D.; Moore, G. F. *J. Am. Chem. Soc.* **2013**, *135*, 11861–11868.